**Title**
High-Definition Single-Cell Printing: Cell-by-Cell Fabrication of Biological Structures



**Journal**
Advanced Materials, 32(52)

**ISSN**
0935-9648

**Authors**
Zhang, Pengfei
Abate, Adam R

**Publication Date**
2020-12-01

**DOI**
10.1002/adma.202005346

Peer reviewed

HHS Public Access

Author manuscript

*Adv Mater*. Author manuscript; available in PMC 2021 December 01.

Published in final edited form as:

*Adv Mater*. 2020 December ; 32(52): e2005346. doi:10.1002/adma.202005346.

# High definition single cell printing: Cell-by-cell fabrication of biological structures

**Pengfei Zhang**,

Department of Bioengineering and Therapeutic Sciences, University of California, San Francisco, San Francisco, CA 94158 USA

**Adam R. Abate**

Department of Bioengineering and Therapeutic Sciences, University of California, San Francisco, San Francisco, CA 94158 USA

California Institute for Quantitative Biosciences, University of California, San Francisco, San Francisco, CA 94158 USA

Chan Zuckerberg Biohub, San Francisco, CA 94158 USA

## Abstract

Bioprinting is a powerful technology with the potential to transform medical device manufacturing, organ replacement, and the treatment of diseases and physiologic malformations. However, current bioprinters are unable to reliably print the fundamental unit of all living things, single cells. Here, we present high definition single cell printing, a novel microfluidic technology that can accurately print single cells from a mixture of multiple candidates. Our bioprinter employs a highly miniaturized microfluidic sorter to deterministically select single cells of interest for printing, achieving an accuracy of ~10 μm and speed of ~100 Hz. We demonstrate this approach by fabricating intricate cell patterns with pre-defined features through selective single-cell printing. We use the approach to synthesize well-defined spheroids with controlled composition and morphology. The speed, accuracy, and flexibility of our approach will advance bioprinting to enable new studies in organoid science, tissue engineering, and spatially targeted cell therapies.

## Graphical Abstract

Conventional bioprinting methods cannot reliably print single cells. A novel microfluidic bioprinting technology with a highly miniaturized cell sorter is presented to accurately print single cells. Through selective cell-by-cell printing, intricate cell patterns at single-cell resolution and uniform spheroids with defined composition and morphology are fabricated.

adam@abatelab.org.

Author contributions

P.Z. and A.R.A designed the research. P.Z. performed the experiments and analyzed the data. P.Z. and A.R.A. wrote the manuscript.

Supporting Information

Supporting Information is available from the Wiley Online Library or from the author.

Competing interests

A.R.A. and P.Z. are inventors on a provisional patent applied by UCSF based on this study.

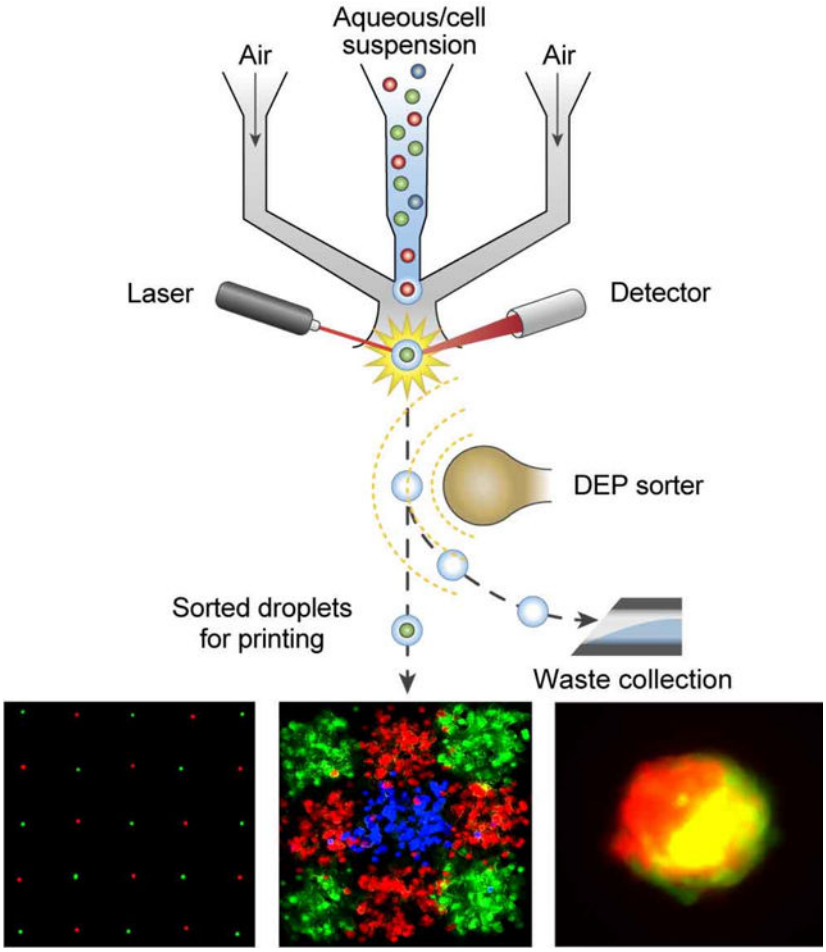


**Keywords**

Single cell printing; droplet microfluidics; fluorescence-activated cell sorting; spheroids; bioprinting

Current approaches to repairing damaged tissues mainly exploit enhancing the body's natural healing properties through physical or pharmaceutical intervention. However, when damage cannot be repaired, the only alternatives are removal or replacement of the tissue. While tissue and organ replacement are essential components for the treatment of numerous health conditions, they can be suboptimal due to the challenges of finding a suitable donor, the possibility of immune rejection, or the need for continuous immune suppression.[1,2] Tissue engineering seeks to create artificial tissues and organs for treatment while also potentially enabling better outcomes, including tissues that function more effectively for longer periods and with less pharmaceutical support.[3] Moreover, if functional structures could be synthesized *in vitro*, replacing damaged tissues and organs would be simpler and more accessible.

Artificial tissue synthesis typically uses "bottom up" methods, in which biological structures are grown from pluripotent cells,[4] or "top down" methods, in which they are built by

physically assembling cells into functional units.[5] Successful examples employ a combination of biological and physical engineering. Bioprinting technologies hold potential for top down synthesis because they can assemble specific building blocks into structures that would be impossible to create with bottom up approaches.[6] For example, bioprinters have successfully constructed ear cartilage, the vascular network of distal lung tissue, and heart replicas, yielding successful clinical and therapeutic outcomes in tissue translation and organ disease modeling.[7–9] Bioprinting also holds potential for *in situ* repair because it can print biomaterials directly onto damaged tissues.[10] Nevertheless, current bioprinters are limited in their ability to control cellular organization.[6,11,12] Like the inkjet bioprinters and laser-assisted bioprinters from which they have descended, bioprinters control the placement of the printed material, but not cells within it.[11,13,14] While bioprinters afford some control over cell density and composition, they cannot precisely control how cells are positioned with respect to each other. Real tissues are structurally and functionally complex over large spatial scales; individual cell types are precisely organized into functional units within large complex structures like tissues and organs.[15] The inability to print structures of densely packed cells with controlled position and composition is thus a major barrier to bioprinting materials mimicking the form and function of real tissues. Even rudimentary assembly of defined structures from accurately printed single cells remains difficult, which limits the production of spheroids, tissue models, and implantable devices in biomedical research, disease treatment, and drug discovery.[16–18] To enable the manufacturing of a new generation of biomaterials with properties mimicking the complexity of biological systems, a new approach for fast and precision single cell printing is needed.

In this paper, we present high definition single cell printing (HD-SCP), a bioprinter to reliably print selected single cells. This is accomplished using a highly miniaturized microfluidic sorter that can select desired single cells from a mixture of candidates and print them with ~10 μm accuracy at a rate of ~100 Hz. The microfluidic printhead is a centimeter in size, and holds potential for scaled up printing through parallelization. To illustrate the ability to construct compact structures, we use the technology to manufacture uniform spheroids of controlled cell number, cell-type ratio, and 3D morphology. To demonstrate the ability to construct extended structures, we print lines, sheets, and 2D image patterns from single cells. Our approach will enable new studies in single cell analysis, organoid science, and tissue engineering through fast and reliable single cell printing.

Current approaches for assembling biological structures with controlled cell-scale properties rely on mediating cell interactions. This can be achieved, for example, using DNA to control cell aggregation,[19] or printing DNA onto substrates to group cells at desired locations.[20] However, constructing complex, multi-layer structures with these approaches has yet to be accomplished. One way to generate elaborate structures from cells would be to combine the flexibility of 3D printing with the cell selectivity of fluorescence activated cell sorting (FACS). However, methods to integrate cell selectivity into bioprinting are unwieldy and slow,[21] while flow cytometers lack the precision to dispense cells with micron resolution.[22] The major challenge limiting accurate cell printing with FACS is its large sorter with charged electrostatic plates, making it impossible to bring the sorter outlet close to the substrate. Hence, the core innovation of HD-SCP is a miniaturized cell sorter that achieves the speed and selectivity of FACS, while being small enough to nearly contact the substrate.

Printed cells travel just ~3 mm from sorter to substrate, affording an accuracy of ~10 μm (Figure 1). By combining this cell sorter with 3D printing components, including a mechanical stage, and controlling the system with a computer, high resolution structures can be printed. Substrate positioning in the x-y plane is controlled by the mechanical stage, allowing the computer to align cell sorting with the substrate. To print a desired structure, we provide the computer with instructions assigning cell-types to each substrate "pixel". The computer moves through the substrate pixel-by-pixel, dispensing the desired cells.

To selectively print cells, the cells are labeled with fluorescent dyes, making them identifiable by flow cytometric measurement.[23] Aerosolization occurs by shearing the cell suspension in a focused air stream, thereby generating monodispersed droplets containing single cells. This design enables uniform droplets with controlled diameters. Varying air and aqueous flow rates, we generate droplets of 36 μm to 50 μm in diameter with a 30 × 30 μm nozzle and 105 μm to 210 μm in diameter with a 70 × 70 μm nozzle (Figure S1a–b, Supporting Information). To characterize the efficacy of the device for printing liquids of different composition, we apply it to liquids with different Ohnesorge numbers (*Oh*), relating liquid viscosity, surface tension, and density.[24] We demonstrate successful printing of liquids with inverse Ohnesorge number (*Z* number) ranging from 0.35 to 34.4 (Figure S1c, Supporting Information). Because we use a co-flow geometry, monodispersed droplets are formed when operating in the "dripping" regime.[25] The wettability of the droplet generator is thus important because it determines wheteher the air shear can lift the aqueous phase from the channel walls and generate a stable dripping cone.[26] We find that hydrophobic channels with a contact angle beyond ~ 40° generate stably dripping cones (Figure S1d, Supporting Information). For surface tensions beyond ~ 24 mN $m^{-1}$, monodispersed droplets are formed with a size that increases with surface tension (Figure S1e, Supporting Information). After generation, the focused air accelerates the droplets past the optical detector that scans them for cells (Figure 2a, right). Fluorescence signals are analyzed in real time by a four-color detector and, based on predefined gating parameters, the cells are sorted. Sorting can thus be thought of as a strategy to deliver specific cells on demand to a given spot, since the cell desired is delivered after selecting it from the mixed suspension.

In conventional flow cytometry, cell sorting is achieved by droplet charging and deflection by an electric field; however, these instruments are unable to achieve enough cell deflection in the compact space required for accurate cell printing.[22,27] Thus, we develop a novel cell sorting mechanism based on dielectrophoresis that exploits the permittivity difference between conductive droplets and the insulating surrounding air.[28,29] Droplet deflection by dielectrophoresis can be tuned by changing applied voltage (Figure S2, Supporting Information). Electrode energization thus allows toggling between deflected (electrode on, Figure 2b) or straight (electrode off, Figure 2c) droplet paths. Because the goal of sorting is to dispense certain droplets and discard all others, deflected droplets must not impact the substrate. To ensure this, we include a vacuum channel downstream of the electrode (Figure 2a, left). The vacuum does not alter the motion of undeflected droplets, but captures deflected ones (Figure 2b, right).

Because dielectrophoretic droplet sorting in air has not been described previously, it is important to quantify accuracy and speed to confirm effectiveness for single cell printing. To quantify sorting accuracy, we capture printed droplets in oil with surfactant; the surfactant stabilizes the droplets, so that they can be imaged after printing, allowing us to quantify rates of false sorts. When droplets are printed irrespective of contents, we observe ~ 10% containing cells, in agreement with the input concentration (Figure 2d). By contrast, when we print only cell containing droplets, > 99.5% contain cells (Figure 2e). Cell printing speed is limited by the time the printer waits for a desired cell to arrive, and thus depends on cell density and the number of different cell types in suspension. At full speed, droplet printing is possible up to ~ 1 kHz (Figure 3a, left, and Movie S1, Supporting Information), four orders of magnitude faster than methods using piezo electric actuation with camera pre-imaging[21]. Beyond this, sorting becomes uncontrolled due to optical and electronic limitations preventing accurate identification of cell type and complete droplet deflection. Substrate repositioning to the next pixel is possible up to ~ 100 Hz with our current mechanical stage. Overall, accurate single cell printing with our current instrument is possible at ~ 50 Hz, at this rate, a 1 cubic millimeter construct consisting of 20 μm cells can be printed in ~ 40 min.

Most biological structures are composed of different components playing distinct roles, such as providing structural support or performing an essential function.[15] If such structures are to be constructed by single cell printing, it is thus necessary to print different cell types. The number of cell types that can be used with our printer depends on the ability to differentiate them by fluorescence. To test this ability, we prepare a suspension with Calcein green stained and Calcein red stained cells. We observe a sorting accuracy of > 98% for green and red cells (Figure 3a, right). Upon inspection, mis-sorts tend to result from limited optical sensitivity causing cell doublets or dim cells of the wrong color to be printed. These results show that we can reliably select and print cells from a mixture, enabling printing of multi-cell patterns.

Most applications of bioprinted structures require that cells remain viable after printing. Cell viability can be harmed by handling and flow through shearing channels. We have designed our sorter to minimize shear, but viability may still be affected. To investigate this, we characterize the viability of cells processed through our printer. We stain cells with live/dead dyes of Calcein Green, AM (live, green) and Ethidium Homodimer-1 (dead, red) (Figure 3b, left) and observe no significant difference in viability for printed or cntrol cells (Figure 3b, right). To determine whether the properties of the suspension phase impact printed cell viability, we test other compositions, but, again, find no difference (Figure S3a, Supporting Information). To determine whether fragile cells are altered, we print hiPSC and primary HSC, but again observe no difference in viability (Figure S3b, Supporting Information). Cell death is the most extreme result of perturbing cells by printing, as a more sensitive test, we measure the secretion of cytokines from printed Jurkat and control cells stimulated with phorbol-12-myristate-13-acetate (PMA), but again find no statistical difference (Figure S3c–d, Supporting Information). To investigate the impact of sorting on proliferation, we culture sorted and control cells and observe their growth (Figure 3c, left), finding all cells have similar growth rates irrespective of sorting (Figure 3c, right). These results illustrate that the sorting process is gentle and does not significantly reduce cell viability or proliferation.

Resolution is a key parameter of any printing technology because it determines the accuracy with which structures can be generated. The main parameter limiting cell printing accuracy is the distance of the cell ejection to the printing substrate. Other approaches for dispensing cells using piezo-electrics or FACS require large instruments that cannot be brought into close contact with the substrate, making them useful only for dispensing cells on large grids.[21,27] By contrast, our miniaturized microfluidic printer can be brought to ~ 3 mm from the substrate, minimizing random drift as cells travel through the air. To quantify printing accuracy, we print Fluorescein isothiocyanate (FITC) stained droplets. We program the device to print arrays of single droplets, five droplets, and spatially varying droplet groups (Figure 4a). Repeated printing to the same spot merges droplets, yielding a larger spot. We calculate the standard deviation of printed droplets with respect to the theoretical position from the printing file, obtaining a mean accuracy of ~ 8 μm for a printing distance of 3 to 5 mm (Figure 4b, and Figure S4a, b, Supporting Information). The printing accuracy is determined by variation in ejection angle from the nozzle, and does not depend on substrate properties (Figure S4c, Supporting Information). At 20 Hz we print an array of 10,000 droplets spaced by 150 μm in ~ 10 min (Figure S4c, Supporting Information).

Printing defined cell combinations on arrays is useful for applications in cell biology and screening, but available bioprinters lack the ability to print cell combinations at precise locations and containing specific numbers of different cell types.[30,31] Our approach can accurately print large and intricate arrays of cells. To illustrate this, we print arrays with alternating green and red cells, and obtain a single cell printing accuracy of ~ 93.25% (Figure 4c, left, and Figure S5a, Supporting Information). By printing one green and one red cell in each spot, we obtain cell pairs with an accuracy of ~ 86.5% (Figure 4c, middle left, and Figure S5b, Supporting Information). More complex arrays can be printed in which conditions systematically vary, such as alternating five cells per spot (Figure 4c, middle right), and linear variation in red and green cell composition (Figure 4c, right).

Although square grids represent the simplest pattern that can be printed with our technology, the mechanical stage can translate through a finer and more complex range of motion, enabling printing of any 2D pattern. To do this, we define a desired “image” by assigning pixels with the type of cell to print. To illustrate this, we print several images extending over centimeters comprising tens of thousands of cells. We first print “UCSF” with the same outline but different cell densities (Figure 4d and Figure S5c, Supporting Information). To print multicolor images, we stain cells with different dyes and print 100-cell squares of different color (Figure 4e). Through layer-by-layer printing of 2D patterns, 3D structures can be generated (Figure 4f). This basic capability allows fabrication of spatially heterogeneous structures composed of controlled cell types. As a final demonstration, we print a ~ 2 mm tall Eiffel Tower from green cells (Figure 4g); the resolution of this image is ~10-fold better than standard inkjet printers.[30]

A key advantage of our single cell printer is that it can print onto any substrate flat enough for close contact of the printhead. Whereas oil-based printers require specialized substrates with integrated electrodes,[23] ours uses air as the surrounding phase and requires no special substrate properties. This makes our printer useful for patterning diverse substrates used in biomedical research and tissue engineering, including tissue culture plastics, cell rafts and

tissues, and nanowell plates. To demonstrate this capability, we construct defined cell clusters in commercially available nanowells (Figure S6, Supporting Information). These results illustrate that our approach can print cells in defined patterns on substrates commonly used in biological research.

Multicellular spheroids provide a physiologic 3D microenvironment and are emerging as useful models for organoid research and building blocks for tissue engineering.[32–34] However, existing methods for generating spheroids lack control.[35] The standard approach is to mix cells in bulk and allow them to randomly aggregate; however, this provides minimal control over composition and generates extremely non-uniform spheroids. Alternatively, uniformity can be increased by aggregating cells in wells and exploiting confinement to constrain assembly.[36] Microfluidic approaches operating on similar principles yield similar results.[37] While better than bulk formation, these approaches provide minimal control over composition since aggregation is random and yields spheroids with random combinations. Moreover, these approaches provide no control over 3D architecture.

The ability to construct spheroids with controlled composition, including numbers of cells, ratios of cell types, and 3D morphology, would represent a significant advance in their manufacturing. It would provide not only high-quality spheroids for research and clinical use, but also the ability to customize their properties. For example, spheroids with specific numbers of distinct cells may respond differently to experimental conditions or drugs, while ones with distinct 3D architecture may better mimic the non-spherical tissues they are intended to model.[38] Because our approach builds structures cell by cell, it provides the control necessary to build spheroids with uniform size, exact numbers and types of cells, and controlled 3D architectures. To illustrate these capabilities, we bioprint spheroids with controlled numbers of starting cells (Figure 5a). We find remarkable uniformity between spheroids printed with the same number of starting cells (Figure 5b and Figure S7a–b, Supporting Information) and that final size is tightly correlated to initial cell count (Figure 5c–d). Indeed, the single cell nature of our printer allows reliable fabrication of spheroids in a manner not previously possible, including from 1, 5 and 10 starting cells (Figure S8a–c, Supporting Information).

Whereas other methods generate spheroids in a random and uncontrolled process, ours builds them cell by cell. This provides new opportunities to control spheroid architecture. To demonstrate this novel capability, we construct spheroids composed of different cell compositions, in which the cells are dispensed in a defined order of first green, then red, and then cultured for 2 days (Figure 5e). The resultant spheroids have non-uniform structure in which the colors tend to aggregate near each other. To make a more extreme structure, we print the green cells on the first day, culture to generate a spheroid, and then print the red cells over one side of the formed spheroid and culture two days (Figure 5f). The resultant spheroid has a Janus-like structure (Figure 5g), which contrasts the irregular spheroids synthesized by passive loading (Figure S9). These results illustrate the potential of using cell-by-cell assembly to construct spheroids with novel architectures. Such systematic investigation of spheroid assembly for different starting conditions has not been possible previously and, thus, there is currently limited understanding of how it affects final structure.

Single cell printing is thus useful as a manufacturing platform for generating controlled spheroids and as a testbed to study how their properties can be engineered by controlling initial cell composition.

Existing bioprinting technologies mainly use extrusion, inkjet or laser induced forward transfer to build structures; while this allows fabrication of intricate structures, it does not provide accurate control over single cells (see Supplementary Discussion for details). Our approach to bioprinting focuses on printing single cells, exploiting the speed and selectivity of fluorescence activated cell sorting. By miniaturizing the printer, we minimize the distance from printhead to substrate and achieve micron resolution printing. Our approach can print any cell type in a pre-defined 2D pattern or 3D spheroid, making it useful for numerous analytical and biomaterial synthesis applications.

Our single cell printer can be used like a flow cytometer to isolate single and multi-cell combinations in grids of spots or wells. Micron resolution allows high density printing into formats currently not supported by commercial sorters, including 1536 well plates, and even denser custom plates. Moreover, such controlled dispensing should afford new opportunities in single cell multi-modal analysis, since printed cells can be subjected to cultivation, imaging, spectroscopy, and array-based single cell sequencing. Indeed, techniques used in flow cytometry should be immediately accessible. For example, cell identification by light scattering, hyperspectral imaging, and real-time imaging would allow identification without the need for pre-labeling. [39–41] While these approaches often fail when applied to unknown populations, our printer uses suspensions of known cell types, making it easier to achieve accurate identification with these label-free methods. Removing the need to fluorescently label cells would simplify the printing workflow and provide greater flexibility in the design of the printed structure.

Our printer affords unique opportunities in biomaterial manufacturing. As we have shown, fast and accurate single cell printing can assemble novel spheroid structures. By including particles and hydrogel matrices, it will be possible to form spheroids with controlled architectures that include voids and functional particles. Spheroids are already a valuable tool in research and drug screening,[32,42] and the ability to construct them reproducibly with advanced features will enable new studies and applications. For example, as we have shown, controlled assembly allows investigation of how starting configuration impacts final structure, which should yield insights into how cells coordinate to generate multicellular structures. Along similar lines, our printer should be compatible eukaryotic and prokaryotic cells. Assembly of these cells should allow investigation of how microbes cooperate to survive in diverse environments, to identify minimally cultivable cell combinations, or study cell interactions in biofilms and the human microbiome.

An intriguing application of our approach is *in situ* cell printing, in which cells or functional particles are directly printed onto living tissue[10]. This is enabled by the small size of the printhead, which allows it to be inserted into constrained spaces and print onto any substrate. As of yet, however, there is little research on how this process could enhance tissue development or healing, because there has never before been such a fast, accurate, and

compact single cell printer. Our platform should thus be useful in advancing this research frontier.

## Supplementary Material

Refer to Web version on PubMed Central for supplementary material.

## Acknowledgements

We are grateful for help from Dr. Kai-Chun Chang with data analysis. We thank Ms. Ivana Vasic from Gladstone Institute for sharing stem cells and Prof. Jennifer Chen from UCSF for sharing primary hepatic stellate cells. We thank Dr. Xiangpeng Li for help with the ELISA assay and helpful discussion. We also thank Dr. Leqian Liu and Dr. Christian A. Silane for helpful discussion. This work was supported by the Chan Zuckerberg Biohub, the National Science Foundation Career Award (Award Number DBI- 1253293), and the National Institutes of Health (Award Numbers 2R01EB019453 and 1DP2AR068129).

## References

[1]. Barnieh L, Collister D, Manns B, Lam NN, Shojai S, Lorenzetti D, Gill JS, Klarenbach S, Clin. J. Am. Soc. Nephrol 2017, 12, 1518. [PubMed: 28818845]

[2]. Halloran PF, Venner JM, Madill-Thomsen KS, Einecke G, Parkes MD, Hidalgo LG, Famulski KS, Am. J. Transplant 2018, 18, 785. [PubMed: 29178397]

[3]. Khademhosseini A, Langer R, Nat. Protoc 2016, 11, 1775. [PubMed: 27583639]

[4]. Ronaldson-Bouchard K, Ma SP, Yeager K, Chen T, Song L, Sirabella D, Morikawa K, Teles D, Yazawa M, Vunjak-Novakovic G, Nature 2018, 556, 239. [PubMed: 29618819]

[5]. Fleischer S, Shapira A, Feiner R, Dvir T, Proc. Natl. Acad. Sci. USA 2017, 114, 1898. [PubMed: 28167795]

[6]. Murphy SV, Atala A, Nat. Biotechnol 2014, 32, 773. [PubMed: 25093879]

[7]. Kang HW, Lee SJ, Ko IK, Kengla C, Yoo JJ, Atala A, Nat. Biotechnol 2016, 4, 312.

[8]. Grigoryan B, Paulsen SJ, Corbett DC, Sazer DW, Fortin CL, Zaita AJ, Greenfield PT, Calafat NJ, Gounley JP, Ta AH, Johansson F, Randles A, Rosenkrantz JE, Louis-Rosenberg JD, Galie PA, Stevens KR, Miller JS, Science 2019, 364, 458. [PubMed: 31048486]

[9]. Lee A, Hudson AR, Shiwarski DJ, Tashman JW, Hinton TJ, Yerneni S, Bliley JM, Campbell PG, Feinberg AW, Science 2019, 365, 482. [PubMed: 31371612]

[10]. Singh S, Choudhury D, Yu F, Mironov V, Naing MW, Acta Biomater. 2020, 101, 14. [PubMed: 31476384]

[11]. Gudapati H, Dey M, Ozbolat IT, Biomaterials 2016, 102, 20. [PubMed: 27318933]

[12]. Ozbolat IT, Hospodiuk M, Biomaterials 2016, 76, 321. [PubMed: 26561931]

[13]. Guillotina B, Souqueta A, Catrosa S, Duocastellab M, Pippengera B, Bellancea S, Bareillea R, Rémya M, Bordenavea L, Amédéea J, Guillemota F, Biomaterials 2010, 31, 7250. [PubMed: 20580082]

[14]. Sun W, Starly B, Daly AC, Burdick JA, Groll J, Skeldon G, Shu W, Sakai Y, Shinohara M, Nishikawa M, Jang J, Cho DW, Nie M, Takeuchi S, Ostrovidov S, Khademhosseini A, Kamm RD, Mironov V, Moroni L, Ozbolat IT, Biofabrication 2020, 12, 022002. [PubMed: 32031083]

[15]. Sasai Y, Nature 2013, 493, 318. [PubMed: 23325214]

[16]. Tasoglu S, Demirci U, Trends Biotechnol. 2013, 31, 10. [PubMed: 23260439]

[17]. Shafiee A, Atala A, Trends Mol. Med 2016, 22, 254. [PubMed: 26856235]

[18]. Murrow LM, Weber RJ, Gartner ZJ, Development 2017, 144, 998. [PubMed: 28292846]

[19]. Qi H, Ghodousi M, Du Y, Grun C, Bae H, Yin P, Khademhosseini A, Nat. Commun 2013, 4, 2275. [PubMed: 24013352]

[20]. Todhunter ME, Jee NY, Hughes AJ, Coyle MC, Cerchiari A, Farlow J, Garbe JC, LaBarge MA, Desai TA, Gartner ZJ, Nat. Methods 2015, 12, 975. [PubMed: 26322836]

[21]. Gross A, Schöndube J, Niekrawitz S, Streule W, Riegger L, Zengerle R, Koltay P, J. Lab. Autom 2013, 18, 504. [PubMed: 24222537]

[22]. Herzenberg LA, Parks D, Sahaf B, Perez O, Roederer M, Herzenberg LA, Clin. Chem 2002, 48, 1819. [PubMed: 12324512]

[23]. Cole RH, Tang SY, Siltanen CA, Shahi P, Zhang JQ, Poust S, Gartner ZJ, R Abate A, Proc. Natl. Acad. Sci. USA 2017, 114, 8728. [PubMed: 28760972]

[24]. Foresti D, Kroll KT, Amissah R, Sillani F, Homan KA, Poulikakos D, Lewis JA, Sci. Adv 2018, 4, eaat1659. [PubMed: 30182058]

[25]. Trebbin M, Krüger K, DePonte D, Roth SV, Chapman HN, Förster S, Lab Chip 2014, 14, 1733. [PubMed: 24671443]

[26]. Rotem A, Abate AR, Utada AS, Van Steijn V, Weitz DA, Lab Chip 2012, 12, 4263. [PubMed: 22864475]

[27]. Picot J, Guerin CL, Le Van Kim C, Boulanger CM, Cytotechnology 2012, 64, 109. [PubMed: 22271369]

[28]. Agresti JJ, Antipov E, Abate AR, Ahn K, Rowat AC, Baret JC, Marquez M, Klibanov AM, Griffiths AD, Weitz DA, Proc. Natl. Acad. Sci. USA 2010, 107, 4004. [PubMed: 20142500]

[29]. Srivastava SK, Gencoglu A, Minerick AR, Anal. Bioanal. Chem 2011, 399, 301. [PubMed: 20967429]

[30]. Park JA, Yoon S, Kwon J, Kim YK, Kim WJ, Yoo JY, Jung S, Sci. Rep 2017, 7, 14610. [PubMed: 29097768]

[31]. Mi S, Yang S, Liu T, Du Z, Xu Y, Li B, Sun W, IEEE Trans. Biomed. Eng 2019, 66, 2512. [PubMed: 30624208]

[32]. Fatehullah A, Tan SH, Barker N, Nat. Cell Biol 2016, 18, 246. [PubMed: 26911908]

[33]. Laschke MW, Menger MD, Trends Biotechnol. 2017, 35, 133. [PubMed: 27634310]

[34]. Eisenstein M, Nat. Methods 2018, 15, 19.

[35]. Brassard JA, Lutolf MP, Cell Stem Cell 2019, 24, 860. [PubMed: 31173716]

[36]. Weber RJ, Cerchiari AE, Delannoy LS, Garbe JC, LaBarge MA, Desai TA, Gartner ZJ, ACS Biomater. Sci. Eng 2016, 2, 1851. [PubMed: 33440521]

[37]. Shin TH, Kim M, Sung CO, Jang SJ, Jeong GS, Lab Chip 2019, 19, 2854. [PubMed: 31367720]

[38]. Au SH, Chamberlain MD, Mahesh S, Sefton MV, Wheeler AR, Lab Chip 2014, 14, 3290. [PubMed: 24984750]

[39]. Rosendahl P, Plak K, Jacobi A, Kraeter M, Toepfner N, Otto O, Herold C, Winzi M, Herbig M, Ge Y, Girardo S, Nat. Methods 2018, 15, 355. [PubMed: 29608556]

[40]. Mehta N, Shaik S, Devireddy R, Gartia MR, J. Biomech. Eng 2018, 140, 020802.

[41]. Ota S, Horisaki R, Kawamura Y, Ugawa M, Sato I, Hashimoto K, Kamesawa R, Setoyama K, Yamaguchi S, Fujiu K, Waki K, Science 2018, 360, 1246. [PubMed: 29903975]

[42]. Arlotta P, Nat. Methods 2018, 15, 27. [PubMed: 29298289]

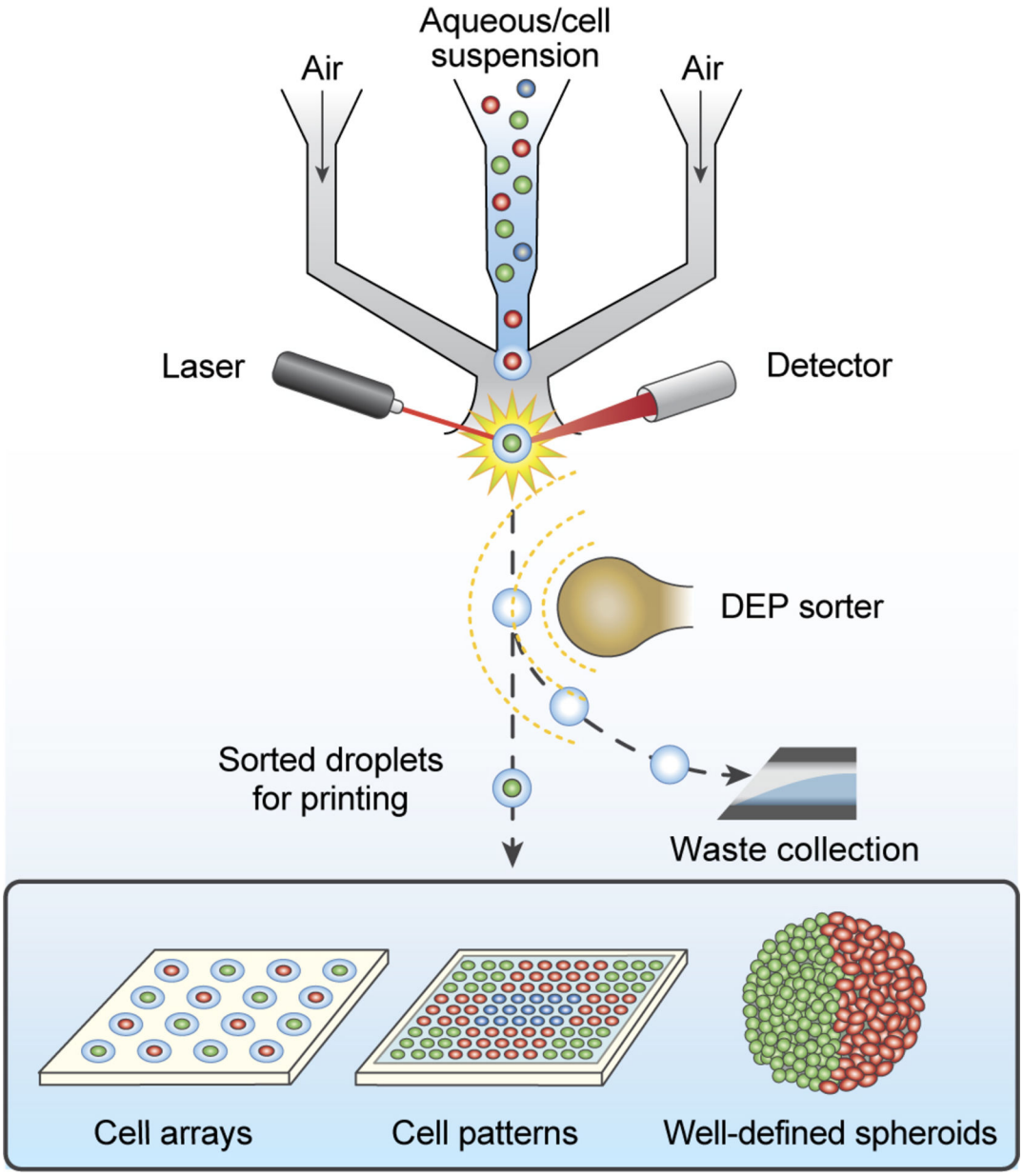


**Figure 1.**

Schematic of HD-SCP printing process. The HD-SCP relies on a microfluidic printhead to eject cell-containing droplets into air, which are subsequently interrogated by a fluorescence-activated sorting system. Droplets with desired single cells are selected through the DEP sorter to print cell arrays, cell patterns, and well-defined spheroids.

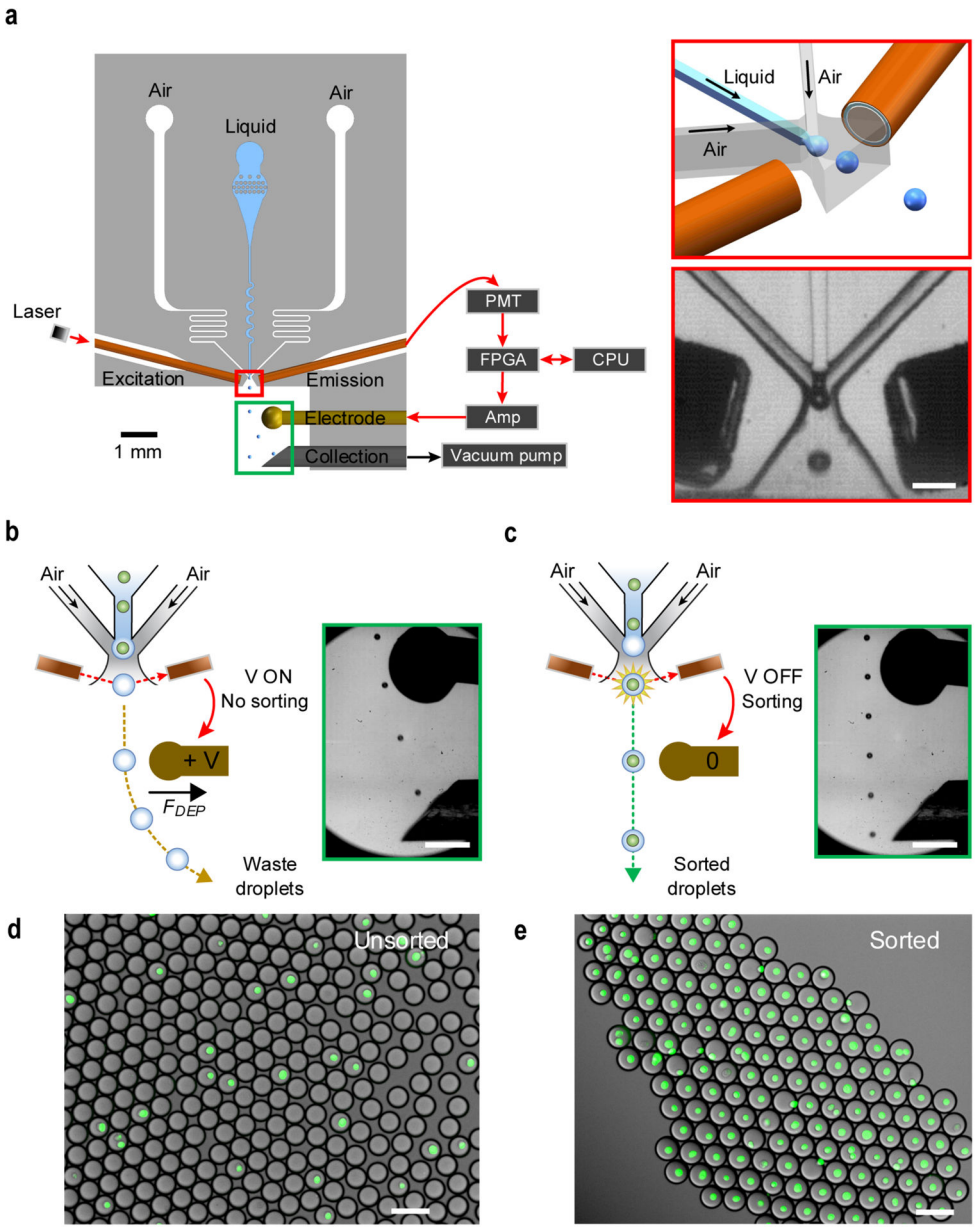


**Figure 2.**

HD-SCP printhead design and operation. a) The HD-SCP printhead integrated with droplet generator, fluorescence droplet sorter, and waste collector modules (left). Droplets are aerosolized by a 3D air/liquid co-flow geometry (right). b) Illustration of waste droplet removal. A constant voltage on the electrode (insert, top) generates a DEP force to deflect droplets into the waste collection tubing (insert, bottom). c) Illustration of sorting process. Detection of a cell of interest by the sorting system triggers an interruption in the voltage on the electrode for a short period to allow the cell to be deposited on the substrate. d) Droplets without sorting follow the Poisson statistic with ~ 10% containing cells. e) Sorted droplets with > 99.5% containing cells. Scale bars represent 100 μm ((a) right, (d), and (e)), and 500 μm ((b) and (c)).

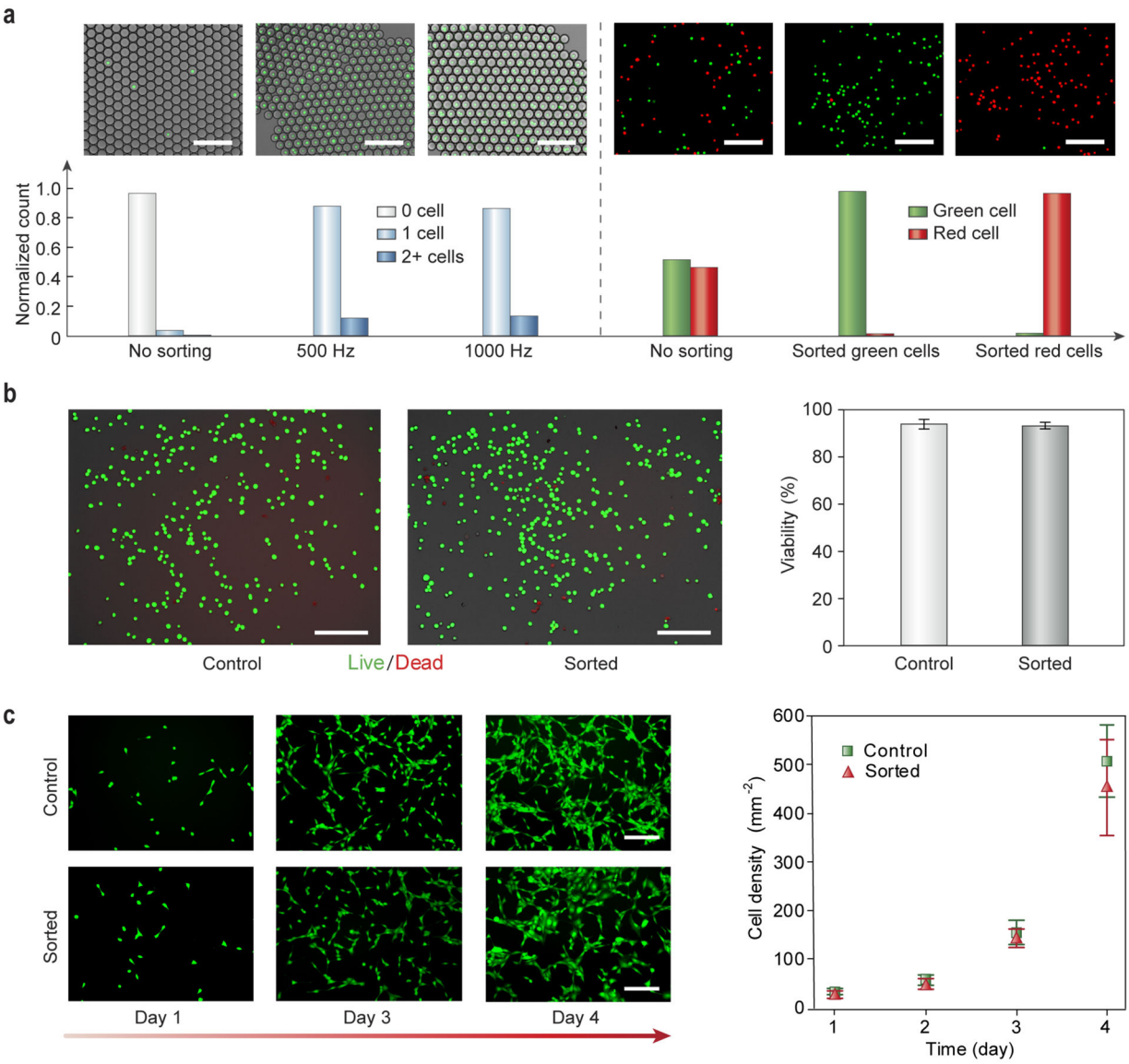


**Figure 3.**

HD-SCP enables single cells sorting with high accuracy and high viability. a) Sorting of cell-containing droplets maintains an accuracy of > 99% across droplet formation frequencies of 500 Hz to 1000 Hz (left, $n$ = 1200 for each condition). Targeted sorting of either Calcein Green stained or Calcein Red stained cells from a mixed population shows an accuracy of > 98% (right, $n$ = 1300 for each condition). Upper insets are corresponding fluorescence images. b) Average cell viability of ~ 94% is observed after sorting, with no significant difference from control cells ($n$ = 5). c) Proliferation assay shows that growth rates over 4 days between sorted cells and control cells are similar ($n$ = 5). Error bars, mean ± s.d. Scale bars represent 200 μm.

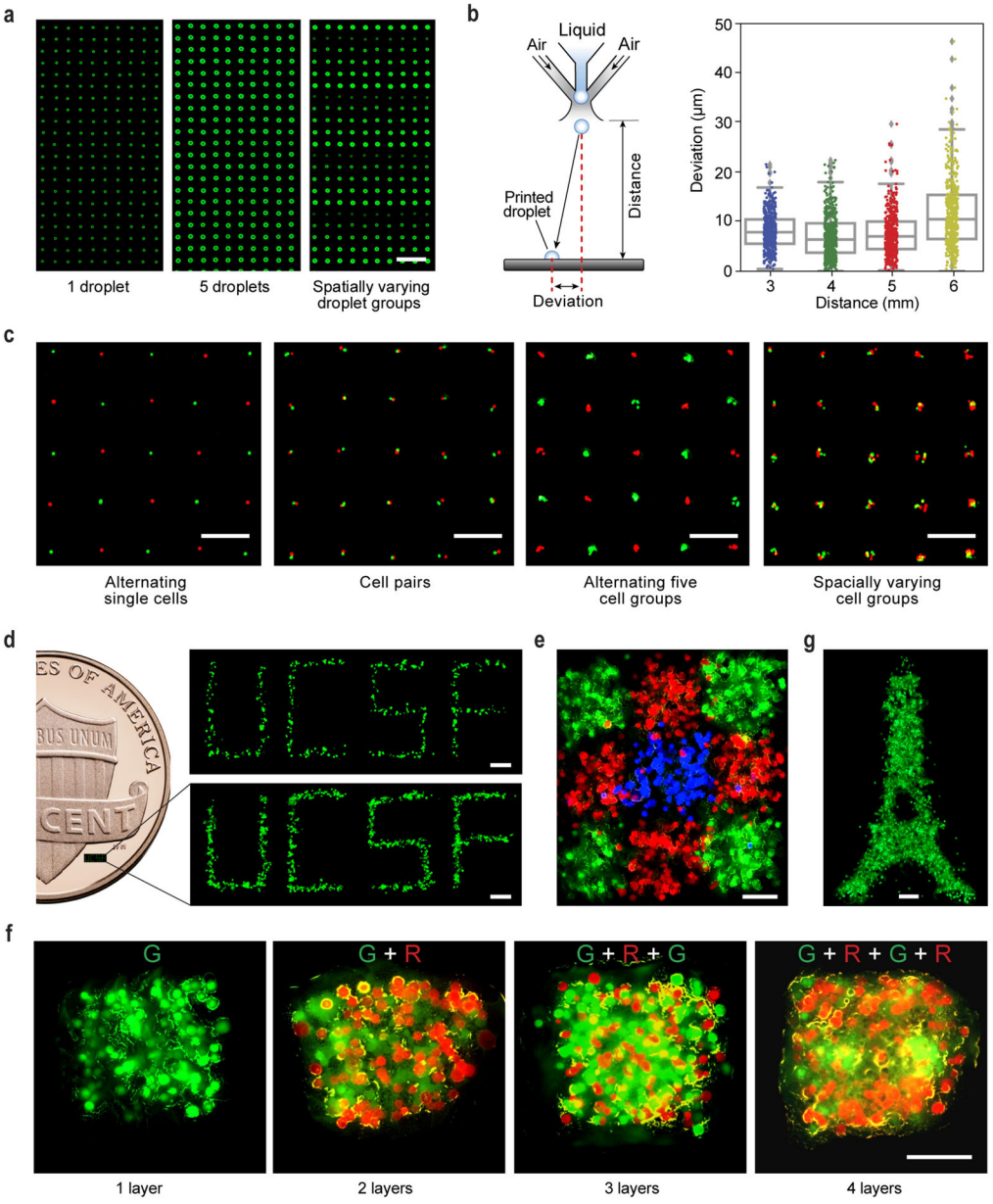


**Figure 4.**

HD-SCP selectively printing of single cells. a) Droplet arrays with one droplet at each position (left), five droplets at each position (middle), and varying one to five droplet groups in a spatial pattern (right) through on-demand printing of FITC stained droplets. b) Measurements of printed droplets show that average printing accuracy is ~ 8 μm when the printing distance is under 6 mm. Boxes represent first to third quartiles and whiskers give 0 – 100% values, excluding the outliers ($n$ = 494 for each condition). c) Cell arrays printed from a mixture of Calcein Green and Calcein Red stained cells. From left to right: alternating single cells, pairs of green and red stained cells, alternating groups of five cells, and cell groups printed based on a spatially varying program (one to five green-stained cells on the vertical axis and one to five red-stained cells on the horizontal axis). d) Patterns of

"UCSF" printed with different cell density from the same bioink with Calcein Green stained cells. The left one-cent coin is a visual reference to show the size of printed patterns. e) Pattern printed from a suspension of Calcein Green, Calcein Red, and CellTrace Far Red (rendered as blue for easily differentiation in the image) stained cells. f) Layer-by-layer printing of structure with alternating layers of green cells and red cells. g) Construction of an "Eiffel Tower" image by printing single cells. Scale bars represent 400 μm ((a) and (c)), 200 μm (d), 100 μm ((e) and (f)), and 200 μm (g).

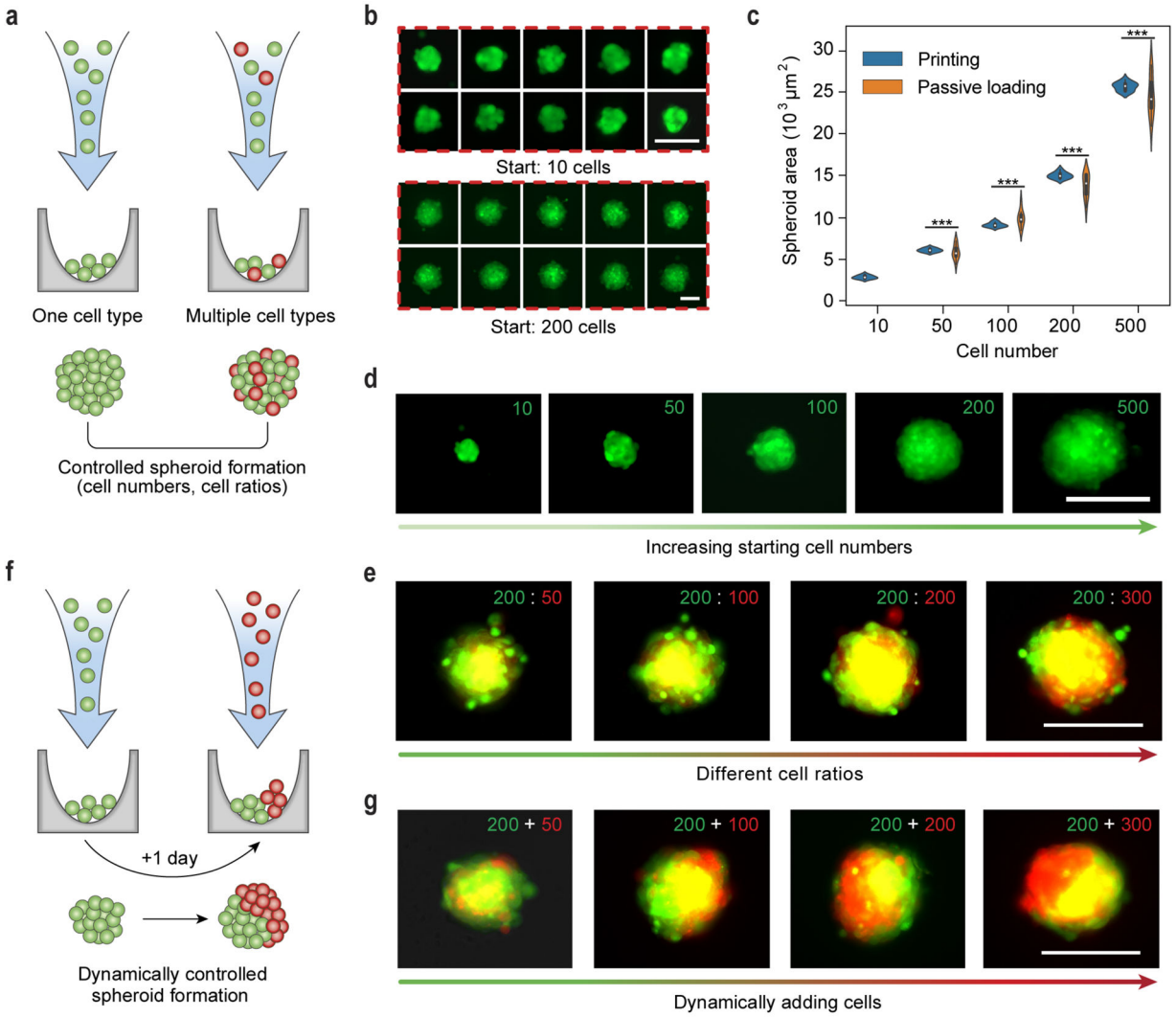


**Figure 5.**

Controlled spheroid formation by HD-SCP. a) Schematic to illustrate controlled spheroid formation through either controlled cell numbers or cell-type ratios. b) Uniform spheroids printed with initial counts of 10 (top) or 200 (bottom) individual cells. c) Violin plot of spheroid size by printing and passive loading. A narrower distribution means a larger uniformity. HD-SCP enables formation of more uniform spheroids over different initial cell counts ($n = 10$ for each condition) compared with passive loading method. ***$p < 0.001$, F test to compare two groups' variances. d) Representative bioprinted spheroids from various starting cell numbers. e) Bioprinted multicellular spheroids from defined starting cell ratios. f) Schematic of dynamically controlled spheroid formation. g) Multicellular Janus spheroids formed by printing 200 cells and then printing various amounts of a second cell-type over one side of formed spheroids after 1-day culture. Scale bars, 100 μm (b) upper, and 200 μm ((b) lower, (d), (e), and (g)).